supported in part by NIH grant HL32303 from the National Heart, Lung and Blood Institute.

References

BLOW, D. M. & ROSSMANN, M. G. (1961). *Acta Cryst.* **14**, 1195-1202.

BLUNDELL, T. L., CUTFIELD, J. F., DODSON, E. J., DODSON, G. G., HODGKIN, D. C. & MERCOLA, D. A. (1971). *Cold Spring Harbor Symp. Quant. Biol.* **36**, 233-241.

BRICOGNE, G. (1976). *Acta Cryst.* A**32**, 832-847.

FAN HAI-FU, HAN FU-SON, QIAN JIN-ZI & YAO JIA-XING (1984). *Acta Cryst.* A**40**, 489-495.

FORTIER, S., MOORE, N. J. & FRASER, M. E. (1985). *Acta Cryst.* A**41**, 571-577.

FUREY, W., ROBBINS, A. H., CLANCY, L. L., WINGE, D. R., WANG, B. C. & STOUT, C. D. (1985). *Science*, **231**, 704-710.

GERMAIN, G., MAIN, P. & WOOLFSON, M. M. (1970). *Acta Cryst.* B**26**, 274-285.

GIACOVAZZO, C. (1983). *Acta Cryst.* A**39**, 585-592.

GREEN, D. W., INGRAM, V. W. & PERUTZ, M. F. (1954). *Proc. R. Soc. London Ser. A*, **225**, 287-307.

HARKER, D. (1956). *Acta Cryst.* **9**, 1-9.

HAUPTMAN, H. (1982*a*). *Acta Cryst.* A**38**, 289-294.

HAUPTMAN, H. (1982*b*). *Acta Cryst.* A**38**, 632-641.

HAUPTMAN, H., POTTER, S. & WEEKS, C. M. (1982). *Acta Cryst.* A**38**, 294-300.

HENDRICKSON, W. A. & TEETER, M. M. (1981). *Nature (London)*, **290**, 107-113.

KARLE, J. (1968). *Acta Cryst.* B**24**, 182-186.

KARLE, J. (1984). *Acta Cryst.* A**40**, 4-11.

KARLE, J. (1985). *Acta Cryst.* A**41**, 387-394.

KARLE, J. & KARLE, I. L. (1966). *Acta Cryst.* **21**, 849-859.

KROON, J., SPEK, A. L. & KRABBENDAM, H. (1977). *Acta Cryst.* A**33**, 382-385.

LANGS, D. A. (1985). *Acta Cryst.* A**41**, 578-582.

PEERDEMAN, A. F. & BIJVOET, J. M. (1956). *Acta Cryst.* **9**, 1012-1015.

PLETNEV, V. Z., GALITSKII, N. M., SMITH, G. D., WEEKS, C. M. & DUAX, W. L. (1980). *Biopolymers* **19**, 1517-1534.

RAMACHANDRAN, G. N. & RAMAN, S. (1956). *Curr. Sci.* **25**, 348-351.

SIM, G. A. (1960). *Acta Cryst.* **13**, 511-512.

WANG, B. C. (1981). *Acta Cryst.* A**37**, C11.

WEEKS, C. M., POTTER, S. A., SMITH, G. D., HAUPTMAN, H. & FORTIER, S. (1984). Am. Crystallogr. Assoc. Meet. 20-25 May 1984, Lexington, Kentucky, USA. Abstr. Q2.

WOOLFSON, M. M. (1984). *Acta Cryst.* A**40**, 32-34.

Acta Cryst. (1986). A**42**, 368-380

Space-Group Analyses of Thin Precipitates by Different Convergent-Beam Electron Diffraction Procedures

BY J. M. HOWE

Department of Metallurgical Engineering and Materials Science, Carnegie-Mellon University, Pittsburgh, PA 15213, *USA*

M. SARIKAYA

Department of Materials Science and Engineering, University of Washington, Seattle, WA 98195, *USA*

AND R. GRONSKY

Materials and Molecular Research Division, Lawrence Berkeley Laboratory, and Department of Materials Science and Mineral Engineering, University of California, Berkeley, CA 94720, *USA*

(*Received* 23 *August* 1985; *accepted* 7 *April* 1986)

Abstract

Convergent-beam electron diffraction point- and space-group analyses were performed on thin γ' precipitate plates, which had been extracted from an Al-15 wt% Ag alloy aged for either 30 or 120 min at 623 K. Although the space groups of precipitates in both samples were determined to be $P6_3/mmc$, it is shown that different results can be obtained, depending on the method of convergent-beam electron diffraction analysis that is employed. Comparative analyses using a pure α-titanium standard demonstrate that the limited thickness of the plate-shaped precipitates is responsible for the variable results, suggesting a preferred method for point- and space-group determination of thin particles.

1. Introduction

Howe & Gronsky (1985) recently demonstrated that symmetry determinations performed on thin specimens by convergent-beam electron diffraction (CBED) may reflect the limited thickness of the specimen along the electron-beam direction, rather than the actual space group of the material. This is a particularly important effect in materials science, where many of the microconstituents which strongly influence the properties of engineering materials are

0108-7673/86/050368-13$01.50

© 1986 International Union of Crystallography

only a few hundred Å thick, and dynamical diffraction is limited.

This article reports the results of space-group determinations that were performed on thin (<300 Å) γ' precipitate plates in an Al–Ag alloy by CBED. Because these plates require both chemical and structural changes for growth, it was hoped that CBED could be used to follow any symmetry or lattice-parameter changes which might occur during the early stages of the growth process. Unfortunately, owing to the limited thickness of the γ' precipitates, difficulties were encountered which prevented complete determination of some of these factors. Because of these difficulties, both space-group and lattice-parameter determinations were performed on a pure α-titanium standard for comparison. In order to achieve the most reliable results, different methods for point-group determination outlined by Buxton, Eades, Steeds & Rackham (1976), Steeds & Vincent (1983) and Tanaka, Saito & Sekii (1983) were compared, as were different methods for space-group determination outlined by Goodman (1975) and Tanaka, Sekii & Nagasawa (1983).

Pure α-titanium was chosen as a standard material because it has similar lattice parameters, average atomic scattering factor and space group to those anticipated for the γ' precipitates. In order to clarify the presentation of the CBED results, the complete space-group and lattice-parameter determinations for the α-titanium are shown first, followed by the results from the extracted precipitates.

2. Experimental

An aluminium alloy containing 14·92 wt% Ag (4·2 at.% Ag) was vacuum melted and cast using Al and Ag of 99·99% purity. The ingot was subsequently homogenized at 808 K for about 40 h to reduce segregation and then hot and cold rolled to about 175 μm final thickness. Several 12 × 12 mm pieces of the sheet were solution-annealed for 30 min at 823 K, quenched in cold water and then aged for 10, 30 or 120 min at 623 K, followed by a final cold-water quench. The γ' precipitates were extracted from each of these sheets by dissolving the matrix in a 5% NaOH solution and dispersing the precipitates in CH_3OH. A small amount of the CH_3OH was then collected in an eye dropper and a drop or two deposited on a carbon film, leaving the γ' plate-shaped precipitates face down for analysis.

Hot-rolled 0·8 mm thick 99·99% Ti sheet was ground to approximately 125 μm thickness on water-cooled SiC papers. Discs 3·0 mm in diameter were punched, vacuum encapsulated and annealed for 1 h at 873 K to produce a completely recrystallized α-phase microstructure. Thin foils were prepared by polishing the discs in a twin-jet Fischione apparatus using a 25% HNO_3/75% CH_3OH electrolyte at about 238 K, with an applied potential of about 50 V and a current of 50 mA.

All of the CBED experiments were performed on a Philips EM400 analytical microscope operating at 100 keV, and equipped with an external circuit so that the objective lens (OL) and second condenser lens (C2L) currents could be independently controlled to achieve a wide range of incident-probe diameters (~100–300 Å) and convergence angles (~10–30 mrad) on the specimens (Sarikaya & Thomas, 1984). In order to utilize fully the information present within the zero-order Laue zone (ZOLZ) CBED discs, the first condenser lens (C1L) was set at the highest excitation (smallest probe diameter) and then the OL current was increased so that the diffraction discs in the ZOLZ just touched without overlapping, while independently focusing the probe on the sample with the C2L 'free control'. Tilting experiments were performed by translating the C2L aperture (equivalent to a gun tilt), after first having obtained a zone-axis (ZA) pattern. A 300 μm C2L aperture and a 450 mm camera length were usually used to photograph the intensity distributions within the ZOLZ discs, while a 100 μm C2L aperture and a 280 mm camera length were employed for photographing the first-order Laue zone (FOLZ). A double-tilt liquid-nitrogen-cooled specimen holder (temperature = 85 K) was utilized to eliminate contamination and reduce thermal diffuse scattering in the specimens, which then produced sharp CBED patterns.

3. Results

3.1. *Examination of space group and lattice parameters of α-titanium*

In its α-phase form, Ti has a hexagonal close-packed structure with $a = 2{\cdot}95030$ and $c = 4{\cdot}68312$ Å (Boyer & Gall, 1985) and is centrosymmetric, with the space group $P6_3/mmc$. All of the CBED pattern symmetry elements for this space group have been derived by Goodman (1975). In addition, Goodman & Whitfield (1980) have performed a complete CBED space-group analysis for GaS, which also has the space group $P6_3/mmc$. The same protocol was followed for determining the space groups of both the α-titanium and extracted precipitates in the present study.

The CBED map of α-titanium in Fig. 1 shows the relationship among the zone axes used in these analyses. The zone axes of interest are the [0001] principal zone and the $[1\bar{1}04]$, $[1\bar{1}02]$ and $[3\bar{3}02]$ zones, all of which are reached by rotating the specimen about $\langle 11\bar{2}0\rangle$.

Fig. 2 shows several CBED patterns obtained from the [0001] principal zone, with the discs in the ZOLZ indexed. Notice that both the whole-pattern (WP) and the bright-field (BF) discs in the ZOLZ patterns

shown in Figs. 2(*a*) and (*b*) have 6*mm* symmetry. That is, they possess six-fold rotational symmetry about an axis which lies in the center of the BF disc [asterisk in Fig. 2(*a*)] and runs perpendicular to the plane of the figures (electron-beam direction). These patterns also contain two mirror lines oriented horizontally and vertically in the figures. Also notice that the FOLZ shown in Fig. 2(*c*) displays the same 6*mm* symmetry. Reference to columns 6 and 7 in Table 2 of Buxton *et al.* (1976) shows that the only two diffraction groups in which both the BF disc and WP display 6*mm* symmetry are 6*mm* and $6mm1_R$.

Column 4 in Table 2 of Buxton *et al.* (1976) shows that it is possible further to distinguish between the diffraction groups 6*mm* and $6mm1_R$ by examining the symmetry present within a dark-field (DF) disc when it is located at a 'special' position in the pattern. In this case, a $\bar{1}010$-type disc located at its Bragg position on one of the mirror lines in the pattern is in a 'special' position, and thus will display only *m* symmetry if the diffraction group is 6*mm*, but will display 2*mm* symmetry if the diffraction group is $6mm1_R$, and provided that HOLZ effects contribute to the dynamical intensities. Also notice from column 6 in Table 2 that these two diffraction groups can be further distinguished by comparing the intensity distributions between ±**g** pairs of $\bar{1}010$-type discs when they are set at their respective Bragg positions. These pairs of discs will be related by a 180° rotation, *i.e.* 2, if the diffraction group is 6*mm*, but will be related by a 180° rotation where the detail within each disc also contains inversion symmetry, *i.e.* 21_R, if the diffraction group is $6mm1_R$. This latter operation is equivalent to a translation operation between the ±**g** discs.

Figs. 3(*a*) and (*b*) show the intensity distributions within the $\bar{1}010$ and $10\bar{1}0$ discs when they are set at their respective Bragg positions. Notice that the detail within each of these discs displays 2*mm* symmetry as indicated in the figures, and that the detail between the discs is related by a translation operation. Therefore, the diffraction group of α-titanium is $6mm1_R$, and the point group of this material can then be determined by referring to Table 3 in Buxton *et al.* (1976). By locating the diffraction group for the [0001] ZA in the left column of Table 3, moving across this row to the X and then following this column down to the bottom row, one finds that the point group of α-titanium is $6/mmm$, which is correct for the space group $P6_3/mmc$. Notice that if a similar analysis is performed by reference to Table 2 in Steeds & Vincent (1983) with the use of Table 2 in Buxton *et al.* (1976) for the ±**g** or DF symmetries, the same point group is obtained for the α-titanium sample.

Tanaka, Saito & Sekii (1983) have introduced a slightly different method for determining the diffraction group of a crystal. Their method uses the detail within all the discs in a single or pair of symmetric many-beam (SMB) patterns in order to obtain the diffraction group. Fig. 3(*c*) shows a six-beam pattern

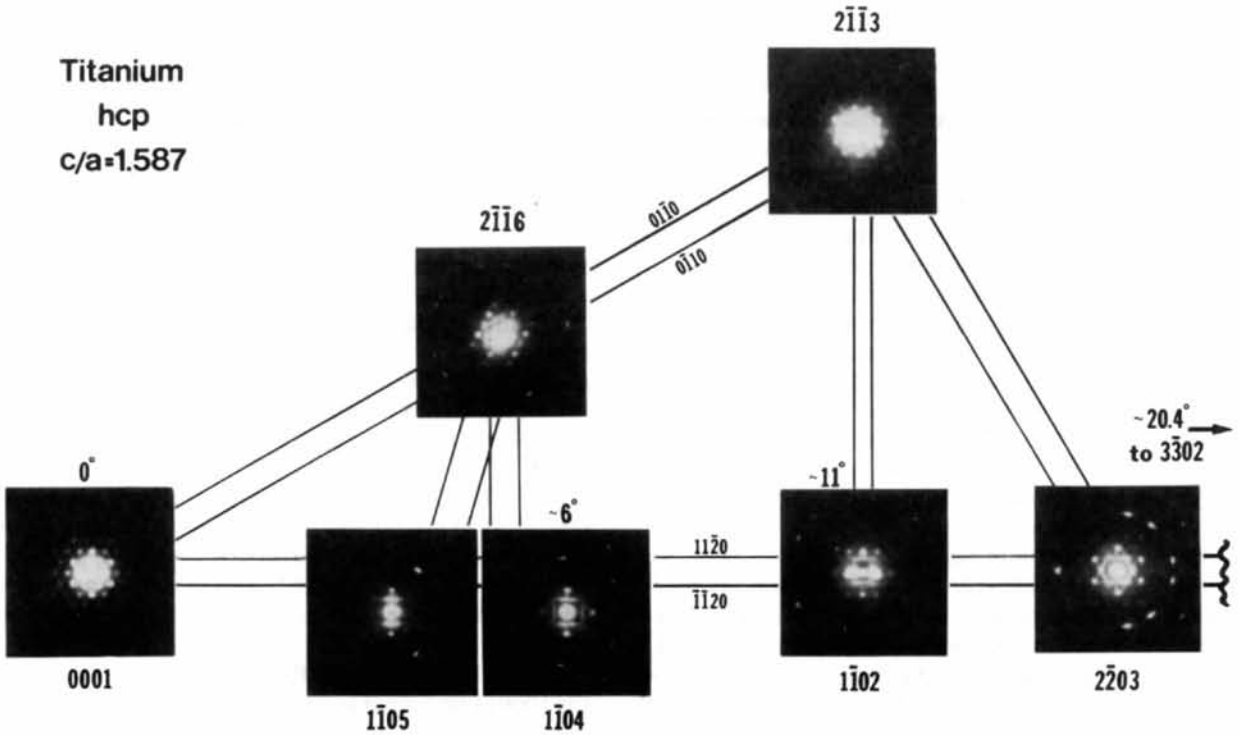

Fig. 1. Partial CBED map for α-titanium around the [0001] principal zone.

from the Ti sample, where the incident beam has been tilted such that the $\bar{1}010$ disc is now centered on the optic axis with the 0000 and $\bar{2}020$ discs positioned symmetrically on either side. The diffraction group of Ti can be determined directly from this pattern by comparing the detail within the six CBED discs in Fig. 3(*c*) with the symmetries in the discs in Fig. 3 of Tanaka, Saito & Sekii (1983) and with Table 3 in the same article. Notice that the $\bar{2}020$ disc in Fig. 3(*c*) displays $2mm$ symmetry as indicated in the figure, and that the 0000 disc and four remaining excited discs surrounding the optic axis all have m symmetry. Also notice that the mirror lines in these discs cross the center of the $\bar{2}020$ diffracting disc. According to the notation in Fig. 3 of Tanaka, Saito & Sekii (1983), the **0** and **G** discs correspond to the 0000 and $\bar{2}020$ (or 2**g**) discs in Fig. 3(*c*). Examination of the symmetries in the **G** discs in Fig. 3 of Tanaka, Saito & Sekii (1983) shows that the only diffraction group which contains $2mm$ symmetry is $6mm1_R$, in the lower-right corner. In addition, notice that the **0** disc and four remaining discs in Fig. 3 of Tanaka, Saito & Sekii (1983) all possess m symmetry, where the mirror lines intersect the center of the **G** disc, just as in Fig. 3(*c*). Thus, it is possible to conclude that the diffraction group of α-titanium is $6mm1_R$ by comparing the single six-beam pattern in Fig. 3(*c*) with the schematic many-beam patterns in Fig. 3 of Tanaka, Saito & Sekii (1983). The point group is then found to be $6/mmm$ from Table 3 in Buxton *et al.* (1976) by following the same procedure as above. Hence, the Buxton *et al.* (1976) and Tanaka, Saito & Sekii (1983) methods for point-group determination give identical results for the α-titanium sample. The same features can also be seen by inspecting the SMB pattern for GaS (space group $P6_3/mmc$) in Fig. 3(*b*) of Goodman & Whitfield (1980), although these authors did not use these features in their analyses. Also notice that the mirror lines in the $\bar{1}010$-type discs in Fig. 3(*c*) are spaced at 30° intervals around the pattern.

Analysis of mirror lines is further investigated in Fig. 3(*d*), where a different many-beam pattern was

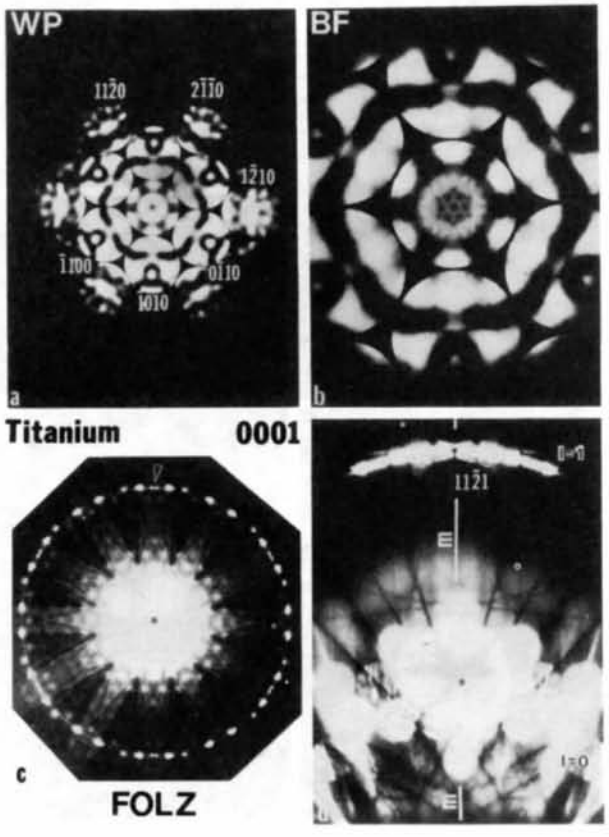

Fig. 2. CBED patterns for α-titanium in a [0001] orientation showing: (*a*) $6mm$ symmetry of the intensity fringes within the ZOLZ discs, (*b*) detail with the BF disc, (*c*) sixfold symmetry of the FOLZ, and (*d*) GM line in the $11\bar{2}1$-type FOLZ reflection at the Bragg position. The location of the optic axis is indicated by an asterisk in these and all subsequent CBED patterns.

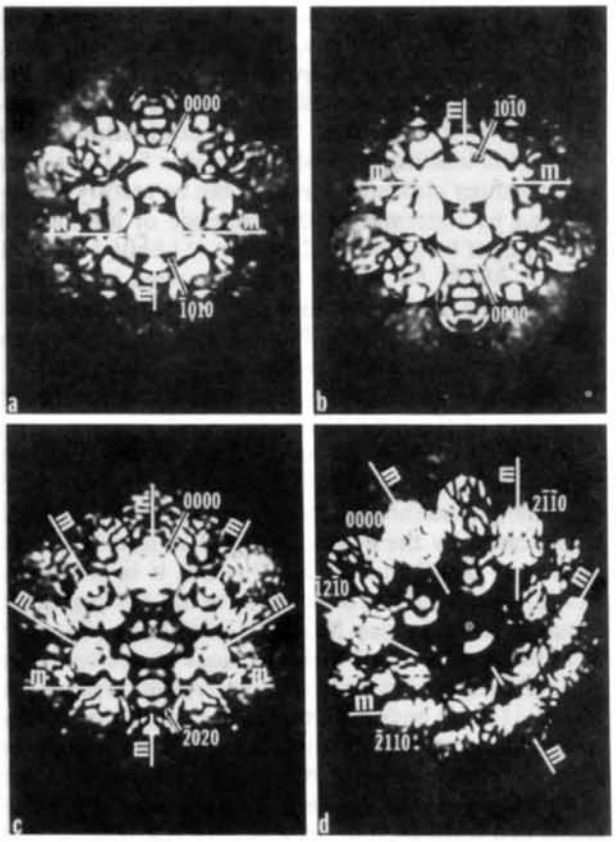

Fig. 3. CBED patterns for α-titanium in a [0001] orientation showing: (*a*) and (*b*) $2mm$ symmetry within the $\bar{1}010$ and $10\bar{1}0$ discs located at their Bragg positions, respectively, (*c*) mirror lines in the six-beam pattern with the $\bar{1}010$ reflection centered on the optic axis (asterisk), and (*d*) symmetric excitation of the $\bar{1}2\bar{1}0$ and $2\bar{1}\bar{1}0$ reflections with mirror lines in all the $11\bar{2}0$ (and $\bar{1}010$-type) discs spaced at 30° intervals.

Table 1. *Summary of forbidden reflections for space groups Nos.* 191–194

Space group (No.)	Kinematically forbidden reflections
$P6/mmm$ (191)	None
$P6/mcc$ (192)	$hh\bar{0}l$, $l=2n+1$ and $hh2\bar{h}l$, $l=2n+1$
$P6_3/mcm$ (193)	$hh\bar{0}l$, $l=2n+1$
$P6_3/mmc$ (194)	$hh2\bar{h}l$, $l=2n+1$

obtained for the Ti sample by tilting the incident electron beam about the $\langle\bar{1}100\rangle$ axis such that the $2\bar{1}\bar{1}0$ and $\bar{1}2\bar{1}0$ reflections are equally excited. Notice that the mirror lines which bisect all of the $11\bar{2}0$-type discs indicated in the figure are also spaced at 30° intervals around the pattern. This feature indicates the presence of horizontal twofold axes at intervals of 60° around the [0001] ZA, parallel to the $\langle11\bar{2}0\rangle$ directions, as shown in Fig. 3 of Goodman (1975) and Fig. 6(*d*) of Goodman & Whitfield (1980).

The space group of α-titanium can now be determined by identifying the presence of kinematically forbidden reflections in the CBED patterns. There are only four space groups which have $6/mmm$ symmetry: $P6/mmm$, $P6/mcc$, $P6_3/mcm$ and $P6_3/mmc$, which appear as space-group nos. 191 through 194 in Vol. I of *International Tables for X-ray Crystallography* (Henry & Lonsdale, 1969). Examination of the conditions limiting possible reflections for these four space groups indicates that they can be readily distinguished by determining the presence or absence of two types of forbidden reflections: (1) $hh\bar{0}l$, $l=2n+1$ and (2) $hh2\bar{h}l$, $l=2n+1$. As summarized in Table 1, space group $P6/mmm$ does not have any forbidden reflections, space groups $P6/mcc$ and $P6_3/mcm$ both contain forbidden reflections of the type $hh\bar{0}l$, $l=2n+1$, while space group $P6_3/mmc$ has a forbidden reflection of the type $hh2\bar{h}l$, $l=2n+1$.

In Fig. 2(*c*), each of the discs which are centered between the pairs of $\langle11\bar{2}0\rangle$ Kossel lines in the FOLZ has a dark band through its center. One of these bands is indicated by the arrow in Fig. 2(*c*) and is shown in greater detail in Fig. 2(*d*), where it is set at the Bragg position. These dark bands or lines of negligible intensity are Gjønnes–Moodie (GM) lines (Gjønnes & Moodie, 1965) and their presence is due to either glide planes or screw axes in the crystal. Gjønnes & Moodie (1965) have determined the conditions under which kinematically forbidden reflections remain at zero intensity when dynamic interactions are included. In the case where the forbidden reflection is due to a vertical glide plane and HOLZ interactions are included, the lines of dynamical absence are present when the incident beam lies in the plane defined by the reciprocal-lattice vector of the forbidden reflection and the axis of projection. This condition is satisfied for the $11\bar{2}1$-type reflections in Figs. 2(*c*) and (*d*), indicating that they are due to a *c*-glide plane parallel to the electron-beam direction. Thus, reflections of the type $11\bar{2}1$ or $hh2\bar{h}l$, $l=2n+1$ are forbidden for α-titanium. This eliminates $P6/mmm$ and $P6_3/mcm$ as possible space groups for this material (Table 1).

In order to distinguish between the space groups $P6/mcc$ and $P6_3/mmc$, the sample can be tilted to zone axes where $hh\bar{0}l$, $l=2n+1$ reflections can be tested for dynamic absences. Reflections of this type occur in both the $[3\bar{3}02]$ and $[1\bar{1}04]$ zones, and were examined in this study. These zone axes were reached by tilting the sample along a $\langle11\bar{2}0\rangle$ Kossel line pair, as shown in Fig. 1. The exact $[3\bar{3}02]$ ZA pattern is shown in Fig. 4(*a*). Notice that when opposite $\bar{1}103$-type reflections are set at their respective Bragg positions in Figs. 4(*b*) and (*c*), they display strong intensity fringes and HOLZ effects without evidence of GM lines, indicating that they are not kinematically forbidden, *i.e.* reflections of the type $hh\bar{0}l$, $l=2n+1$ are allowed. Thus reference to Table 1 indicates that the only possible space group for α-titanium is

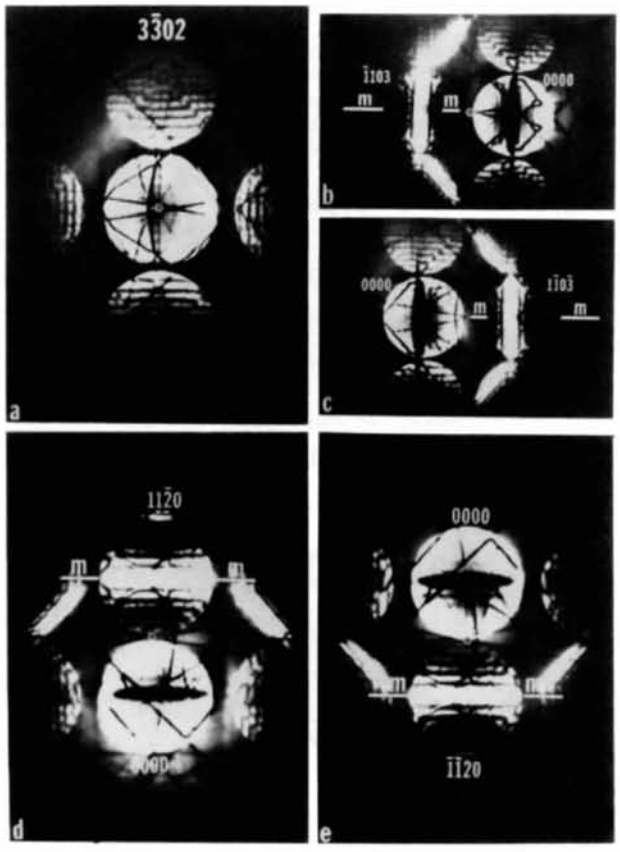

Fig. 4. (*a*) $[3\bar{3}02]$ CBED pattern for α-titanium, (*b*) and (*c*) intensity fringes and HOLZ lines within the $\bar{1}103$ and $1\bar{1}0\bar{3}$ discs at their respective Bragg positions, and (*d*) and (*e*) intensity distributions within the $11\bar{2}0$ and $\bar{1}\bar{1}20$ discs at their respective Bragg positions. The mirror lines are indicated in all of the Bragg reflections, which also display translational symmetry.

$P6_3/mmc$, as expected. Also notice that the detail between the $\bar{1}103$ and $1\bar{1}0\bar{3}$ discs is related by a translation operation (21_R), further verifying the element of centrosymmetry in the crystal (Buxton *et al.*, 1976; Goodman & Whitfield, 1980) that was detected when the $\pm\mathbf{g}$ experiment was performed in the higher-symmetry [0001] ZA. The $11\bar{2}0$ and $\bar{1}\bar{1}20$ discs in Figs. 4(*d*) and (*e*) are also related by a similar translation operation. In addition, notice that the mirrors in these discs are perpendicular to their reciprocal-lattice vectors. This feature indicates the presence of a horizontal twofold rotation axis which is parallel to the $\langle 11\bar{2}0\rangle$ axis in the crystal (Goodman & Whitfield, 1980) as was observed for Figs. 2(*c*) and (*d*), and is strong evidence for the presence of an inversion center in the crystal. Also notice that the $[3\bar{3}02]$ ZA pattern is nearly square. This is different from the highly rectangular $[3\bar{3}02]$ CBED pattern shown in Fig. 3 of Goodman & Whitfield (1980), indicating that they identified the wrong ZA pattern as $[3\bar{3}02]$ in their paper. However, this does not detract from their results.

Fig. 5 shows the $[1\bar{1}04]$ CBED ZA pattern and three four-beam patterns, which were obtained by tilting the incident beam such that it was symmetrically positioned among the four discs, as indicated in the figures. Notice that the intensities within the $\bar{2}201$-type reflections in these patterns are quite strong, and that they do not display evidence of GM lines, further verifying that $hh\bar{0}l$, $l=2n+1$ reflections are not forbidden. Also notice that opposite pairs of both $11\bar{2}0$ and $\bar{2}201$-type reflections in this low-symmetry ZA display translational symmetry as well as the presence of horizontal twofold rotation axes. In addition, the detail within the $\bar{1}32\bar{1}$-type CBED discs nearly has inversion symmetry (1_R), indicating the presence of a horizontal mirror ($/m$) in the crystal, *i.e.* perpendicular to the electron beam (Buxton *et al.*, 1976; Goodman & Whitfield, 1980). Thus, all of the symmetry elements for the space group $P6_3/mmc$ have been directly identified from these CBED patterns, exactly as outlined by Goodman (1975) and performed by Goodman & Whitfield (1980) for GaS, except for the 6_3 screw axis, which can only be identified by examining the specimen in either $\langle 11\bar{2}0\rangle$ or $\langle\bar{1}010\rangle$ orientations, 90° to the $\langle 0001\rangle$ axis. Since it is not possible to obtain these orientations in this foil or in the extracted precipitates which follow because the basal plane is oriented perpendicular to the electron beam, it is not possible to identify the space group of the samples using Table 13 in Tanaka, Sekii & Nagasawa (1983), which requires examination of the GM lines in either a $\langle 11\bar{2}0\rangle$ or $\langle\bar{1}010\rangle$ orientation.

Also notice how much stronger the HOLZ lines are in the $[1\bar{1}04]$ ZA pattern in Fig. 5(*b*) as compared with the $\langle 0001\rangle$ ZA patterns in Figs. 2(*a*) and (*b*), where weak HOLZ lines are barely visible. Kohler, Shelton & Ralph (1983) have shown that the fine HOLZ lines in the $[1\bar{1}04]$ zone axis vary sensitively with the lattice parameters in hexagonal close-packed crystals and therefore can be used to make lattice-parameter measurements which are precise up to 0·1%. In addition, the intersection of the Ewald sphere with the FOLZ in Fig. 2(*c*) leads to a bright ring which can be easily measured to obtain the lattice spacing along the *c* axis with an accuracy of about 1% (Steeds & Vincent, 1983), provided that the microscope is calibrated to minimize errors due to distortion of the ring by the projector lens. The latter measurement was performed in this investigation and the lattice parameter along the *c* direction was determined to be $c=4{\cdot}746$ Å by using the relation: $G=(2KH)^{1/2}$, where $G=$ radius of the FOLZ ring, $K=$ electron wavevector $(1/\lambda)$, $H=$ reciprocal-lattice spacing parallel to the electron beam, and assuming that $d_{\bar{1}010}=2{\cdot}555$ Å. This value for *c* is about 0·2% larger than the value of 4·68312 Å determined by X-ray diffraction (Boyer & Gall, 1985).

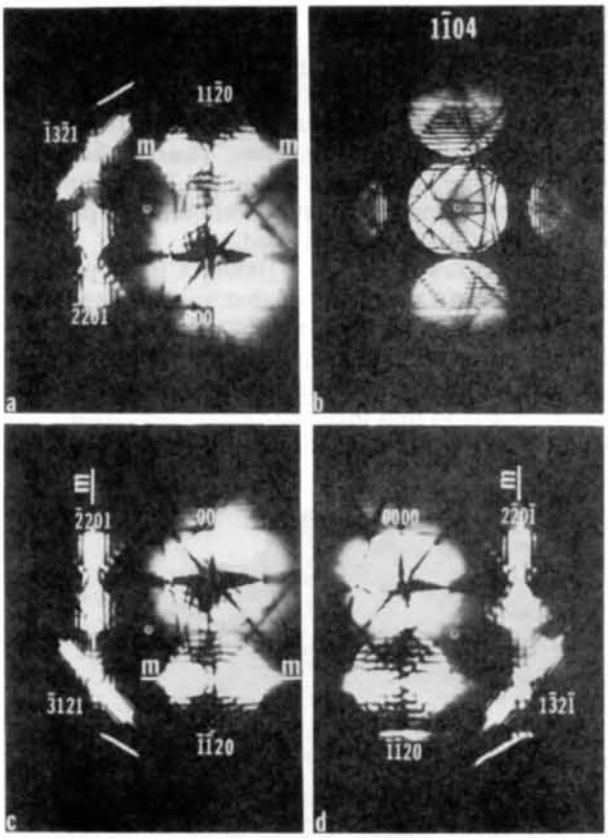

Fig. 5. (*a*), (*c*) and (*d*) Three conjugate four-beam CBED patterns around the $[1\bar{1}04]$ zone axis shown in (*b*). Notice the translational symmetries between opposite CBED reflections and the near-inversion-symmetry within the $\bar{1}32\bar{1}$-type discs in these patterns. Also notice the strong HOLZ lines in the zone-axis pattern in (*b*).

3.2. *Determination of space group and lattice parameter of γ′ precipitates*

Based on the results from the previous analyses for α-titanium, the present section explains the results of similar space-group and lattice-parameter determinations that were performed on the extracted γ′ precipitates. As previously mentioned, these analyses were performed to follow any symmetry or lattice-parameter changes which might occur during the early stages of precipitate growth. However, it was not possible to find any γ′ precipitates which were thick enough to display intensity fringes in the CBED discs for the sample aged for only 10 min at 623 K. In fact, while a number of extracted precipitates could be readily found for analysis in the 120 min sample, only a few precipitates in the 30 min sample were thick enough to display any intensity fringes in the CBED patterns. Hence, the effect of precipitate thickening during aging was directly reflected in the CBED analyses, and only precipitates from samples that were aged for 30 min or longer could be examined. In addition, slight distortion of the intensity distributions within the CBED discs from the extracted precipitates sometimes occurred, because the thin precipitates always bent when irradiated by the electron beam. This bending caused the precipitates to be filled with extinction contours (see Fig. 6 for example), and the probe was placed within these bend contours for the CBED analyses. Thus, if the probe was not entirely contained within the ZA determined by the bend contours, slight distortion of the patterns within the CBED discs resulted.

Fig. 7 shows a series of [0001] CBED patterns obtained from a γ′ precipitate that was extracted from the sample aged for 30 min at 623 K. These patterns can be compared directly with the same series of patterns for the Ti sample in Fig. 2. Although the precipitate is so thin that there is no detail within the BF disc in Fig. 7(*b*), notice that the WP in Fig. 7(*a*) and FOLZ in Fig. 7(*c*) both display 6*mm* symmetry. Thus, reference to Table 2 in Buxton *et al.* (1976) indicates that the diffraction group of the precipitate is either 6*mm* or $6mm1_R$.

Fig. 8 shows another series of ±**g** and tilted-illumination CBED patterns, which may be compared directly with the patterns for the Ti sample in Fig. 3. The $\bar{1}010$ and $10\bar{1}0$ discs at their Bragg positions in Figs. 8(*a*) and (*b*) clearly display only *m* symmetry as indicated in the figures. In addition, these discs are also related by a 180° rotation, rather than by a translation operation. Reference to Table 2 in Buxton *et al.* (1976) thus indicates that the diffraction group for the precipitate which was aged for 30 min at 623 K is 6*mm*, and not $6mm1_R$ as for the previous Ti sample. By using Table 3 in Buxton *et al.* (1976), the point group of the precipitate is then identified as 6*mm*.

If the Tanaka, Saito & Sekii (1983) six-beam CBED pattern in Fig. 8(*c*) is now used to determine the diffraction group of the precipitate instead of the Buxton *et al.* (1976) method above, a different result is obtained. Although the detail within some of the

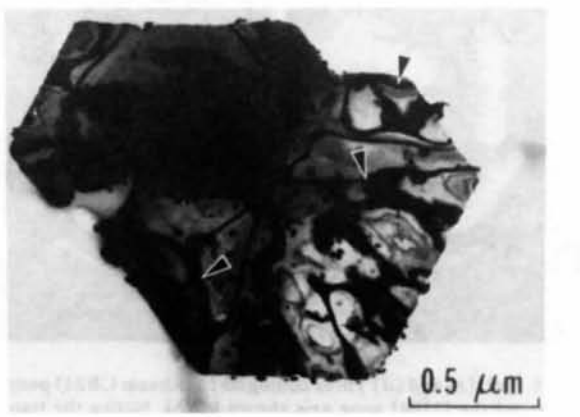

Fig. 6. Bright-field transmission electron microscope image of two γ′ precipitates lying face-down on a carbon film. Notice the bend contours (arrows) present throughout the thin precipitates.

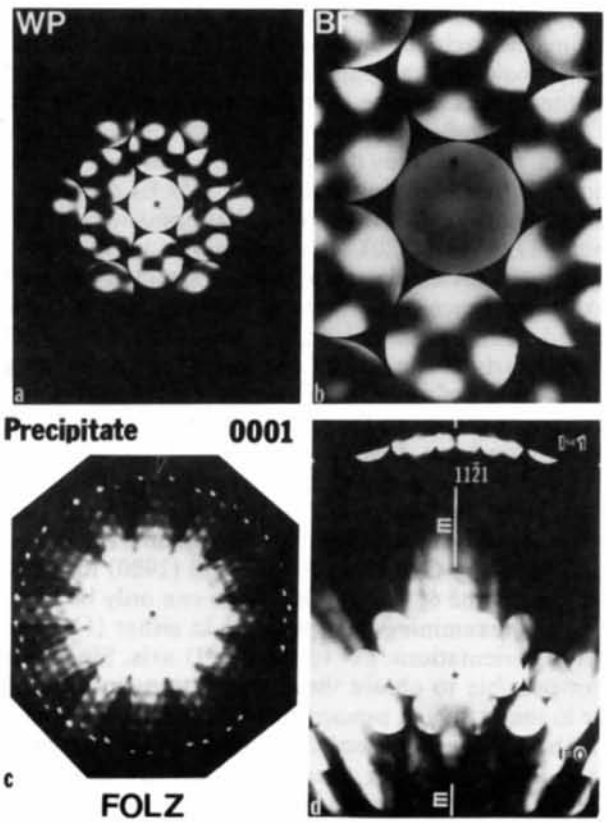

Fig. 7. CBED patterns for extracted γ′ precipitate in a [0001] orientation showing: (*a*) 6*mm* symmetry of the intensity distributions in the ZOLZ discs, (*b*) absence of detail within the BF disc owing to the thinness of the precipitate, (*c*) sixfold symmetry of the FOLZ, and (*d*) GM line in the $11\bar{2}1$-type FOLZ reflection at the Bragg position. As for the Ti sample, the position of the optic axis is indicated by an asterisk in all of the CBED patterns.

CBED discs in the SMB pattern is slightly distorted due to bending of the precipitate, the $\bar{2}020$ disc nearly displays $2mm$ symmetry. In addition, the 0000 disc and four remaining excited discs all have m symmetry as indicated in the figure, where the mirror lines intersect the center of the $\bar{2}020$ disc. Thus, comparison with the SMB patterns in Fig. 3 of Tanaka, Saito & Sekii (1983) indicates that the diffraction group of the precipitate is $6mm1_R$, which is the same as the α-titanium sample in Fig. 3(c). Further reference to Table 3 in Buxton *et al.* (1976) then identifies the point group of the precipitate as $6/mmm$.

According to these results, the Buxton *et al.* (1976) and Tanaka, Saito & Sekii (1983) methods of point-group determination yield two different point groups for the precipitate. Since the Steeds & Vincent (1983) method for point-group determination also relies on comparison between the intensity distributions in $\pm\mathbf{g}$ discs or in a DF disc to distinguish between the $6mm$ and $6mm1_R$ diffraction groups, the result is the same as with the Buxton *et al.* (1976) method. However, because the centrosymmetry *versus* thickness results of Howe & Gronsky (1985) for α-titanium in a $\langle 1\bar{1}02\rangle$ ZA have shown that a loss of translational symmetry between $\pm\mathbf{g}$ discs can occur in thin specimens due only to their limited thickness along the electron-beam direction, it is likely that this effect is responsible for the 180° rotational symmetry observed between the $\bar{1}010$ and $10\bar{1}0$ discs in Figs. 8(a) and (b), particularly since no HOLZ lines are present in the CBED patterns and the precipitate is just thick enough for weak dynamical diffraction to occur. Therefore, it is probable that the precipitate has the higher-symmetry diffraction group given by the SMB pattern in Fig. 8(c) and that its point group is $6/mmm$. Also notice that the mirror planes in both Figs. 8(c) and (d) are spaced at 30° intervals in the patterns, indicating the presence of horizontal twofold rotation axes at 60° intervals around the [0001] ZA, parallel to the $\langle 11\bar{2}0\rangle$ directions, as for the Ti sample.

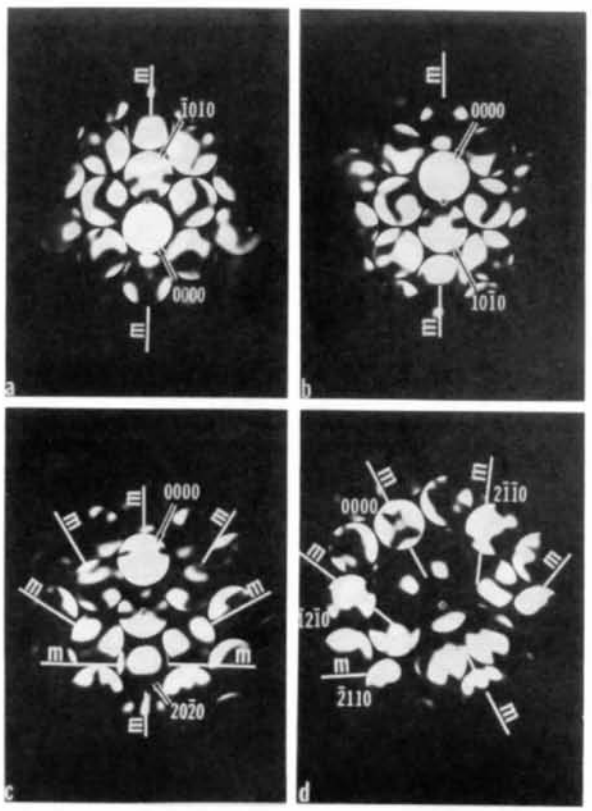

Fig. 8. CBED patterns for extracted γ' precipitate in a [0001] orientation showing: (a) and (b) a single mirror line and 180° rotational symmetry between the $\bar{1}010$ and $10\bar{1}0$ discs located at their Bragg positions, respectively, (c) mirror lines in the six-beam pattern with the $10\bar{1}0$ disc centered on the optic axis (asterisk), and (d) symmetric excitation of the $\bar{1}2\bar{1}0$ and $2\bar{1}\bar{1}0$ reflections with mirrors in all the $11\bar{2}0$ (and $\bar{1}010$-type) discs spaced at 30° intervals.

The space group of the precipitate is further obtained by identifying the presence of forbidden reflections in the CBED patterns. Assuming that the point group of the precipitates is $6/mmm$, the only four possible space groups are those listed in Table 1, which can be distinguished by the presence or absence of forbidden reflections of the type $hh\bar{h}0l$, $l=2n+1$ and $hh2\bar{h}l$, $l=2n+1$. Notice that GM lines are present in the $11\bar{2}1$-type discs in Figs. 7(c) and (d), indicating the presence of $hh2\bar{h}l$, $l=2n+1$ forbidden reflections in the precipitate, exactly as for the α-titanium sample. Thus, the space group of the precipitate must be either $P6/mcc$ or $P6_3/mmc$. Again, these two space groups can be distinguished by tilting the precipitate to $[1\bar{1}02]$ and $[1\bar{1}04]$ zone axes, and examining the detail within $hh\bar{h}0l$, $l=2n+1$ discs.

Fig. 9(a) shows the $[1\bar{1}02]$ ZA CBED pattern. Notice that the overall pattern displays $2mm$ symmetry due to a lack of HOLZ lines, as discussed by Howe & Gronsky (1985). These mirror lines are also present in the two sets of $\pm\mathbf{g}$ pairs shown for the $11\bar{2}0$ and $1\bar{1}01$-type reflections in Figs. 9(b) through (d). In particular, notice that the $\bar{1}101$ and $1\bar{1}0\bar{1}$ discs in Figs. 9(d) and (e) are related by a 180° rotation rather than by a translation operation. This relation was observed between the same pair of discs in thin areas of the α-titanium sample examined by Howe & Gronsky (1985), further indicating that the limited thickness of the precipitate may be responsible for its apparent loss of the $/m$ symmetry element. The limited thickness of the precipitate is evidenced by the lack of detail within these discs due to the weak dynamical diffraction which is occurring. Also notice that there is no evidence of GM lines in the $\bar{1}101$-type discs, indicating that $hh\bar{h}0l$, $l=2n+1$ reflections are allowed for the precipitate and, therefore, that its space group is $P6_3/mmc$, as for the α-titanium sample.

Fig. 10 shows the [1$\bar{1}$04] CBED ZA pattern and three four-beam patterns which can be compared directly with the same series of micrographs for the α-titanium sample in Fig. 5. Notice the resemblance between the detail within the $\bar{2}$201-type discs in Figs. 5 and 10. The strong intensities of these reflections and lack of evidence that they are forbidden further verifies that $hh\bar{0}l$, $l=2n+1$ reflections are allowed for the precipitate, and that its space group is $P6_3/mmc$. In addition, notice that there is almost translational symmetry between opposite $\bar{2}$201 and 11$\bar{2}$0-type reflections in the four-beam patterns, and that these reflections also demonstrate the presence of horizontal twofold rotation axes in the precipitate. Further, the detail within the $\bar{1}3\bar{2}1$-type discs nearly has inversion symmetry (1_R), indicating the presence of a horizontal mirror ($/m$) in the precipitate. Thus, the symmetries obtained from the CBED patterns in this low-symmetry ZA appear to be less sensitive to the limited thickness of the precipitate than the patterns obtained in the previous orientations. The evidence for a center of symmetry and horizontal mirror obtained in this orientation also confirms that the space group of the precipitate is $P6_3/mmc$ and, therefore, that the correct point group is $6/mmm$ as determined by the SMB pattern in Fig. 8(c).

The reason why the [1$\bar{1}$04] ZA reveals the full three-dimensional symmetry in the thinner specimen is probably that HOLZ interactions are stronger in this orientation than in the [0001] and [1$\bar{1}$02] orientations, as evidenced by the presence of faint HOLZ lines within the BF disc in Fig. 10(b). The HOLZ interactions are stronger because the crystal repeat distance along the electron-beam direction is shorter in reciprocal space, leading to greater scattering into HOLZs and increased dynamical diffraction. The increased electron concentration into HOLZs in lower-symmetry zone axes is also evident by comparing the strong HOLZ lines in the BF disc in Fig. 5(b) with those of the BF disc in Fig. 2(b). Therefore, it appears that when the sample is thin along the electron-beam direction the $\pm\mathbf{g}$ experiment which is often required for diffraction-group determination by either the Buxton *et al.* (1976) or Steeds & Vincent (1983) methods is more reliable when performed at low-

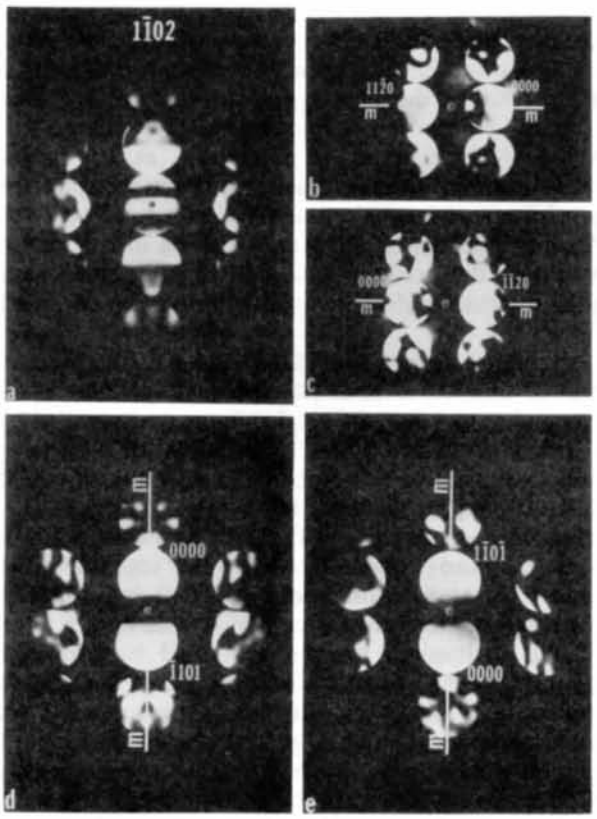

Fig. 9. (a) [1$\bar{1}$02] CBED pattern for γ' precipitate with $2mm$ symmetry, (b) and (c) intensity distributions in the 11$\bar{2}$0 and $\bar{1}$1$\bar{2}$0 discs at their respective Bragg positions, and (d) and (e) intensity fringes within the $\bar{1}$101 and 1$\bar{1}$0$\bar{1}$ discs at their respective Bragg positions. Notice that opposite $\bar{1}$101-type discs in (d) and (e) are related by a 180° rotation.

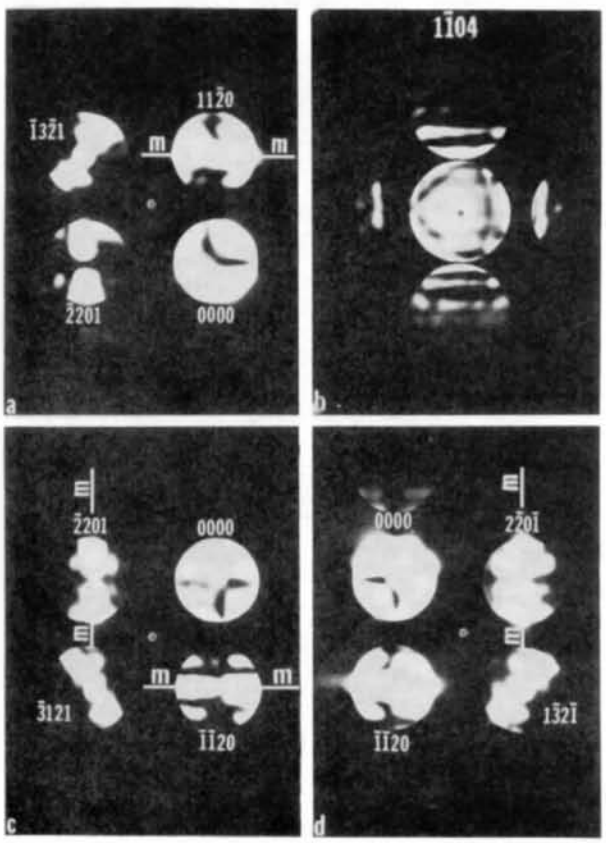

Fig. 10. (a), (c) and (d) Three conjugate four-beam CBED patterns around the [1$\bar{1}$04] zone axis shown in (b). As for the Ti sample, notice the translational symmetries between opposite CBED reflections and the near-inversion-symmetry within the $\bar{1}3\bar{2}1$-type discs in these patterns. Also notice the weak HOLZ lines in the zone-axis pattern in (b).

symmetry zone axes. However, the HOLZ lines in the $[1\bar{1}04]$ BF disc are still not strong enough to obtain accurate lattice-parameter information for the precipitate. Nevertheless, by measuring the diameter of the bright ring in the FOLZ [which is barely visible in Fig. 7(*c*)] and assuming that $d_{\bar{1}010} = 2{\cdot}47$ Å for the γ' precipitate, the lattice spacing along the *c* direction can be determined. Using the equation given above for the titanium sample, a value of $c = 4{\cdot}676$ Å was obtained. This spacing is about 1·5% larger than the value of 4·607 Å usually given for these precipitates (Mondolfo, 1979; Barrett & Geisler, 1940), and is equal to the lattice spacing of two {111} matrix planes, *i.e.* $d_{111} = 2{\cdot}338$ Å. One reason for this spacing may be that the precipitates are less than 200 Å thick and still in the early stages of growth. Therefore, they may not have achieved the full contraction along the *c* direction which is characteristic of latter-stage precipitates. However, Howe, Aaronson & Gronsky (1985) have measured the lattice spacings of the same precipitates by optical diffraction from HREM negatives, and their results showed that there is about a 2·5% contraction among the basal planes in the precipitates when compared with the octahedral matrix planes. Thus, the larger *c* spacing obtained from the CBED pattern is probably due to the error made in measuring the diameter of the FOLZ, since the bright ring associated with the FOLZ is barely visible in the pattern.

Identical space-group analyses and lattice-parameter determinations were also performed on extracted precipitates from the sample that was aged for 120 min at 623 K. The results from one precipitate are shown in Figs. 11 through 13. Since they are almost identical to those just discussed, only the differences between the analyses for the 30 and 120 min precipitates are described.

The [0001] CBED patterns for the 120 min precipitate in Figs. 11 and 12 are similar to those in Figs. 7 and 8, except that detail is present within the BF disc for the precipitate in Fig. 11(*b*). However, notice that the hexagon within the BF disc does not have sixfold rotational symmetry. This is because the electron probe was focused slightly above the specimen when the CBED pattern was taken, and thus the detail is slightly elongated in one direction. Therefore, it can be concluded that the BF disc possesses *6mm* symmetry when the probe is correctly focused, and that the diffraction group of this precipitate is either *6mm* or $6mm1_R$.

Examination of Figs. 12(*a*) through (*c*) again shows that the SMB technique for point-group determination [Fig. 12(*c*)] yields a higher-symmetry point group than the ±**g** technique [Figs. 12(*a*) and (*b*)]. The mirror lines in the six-beam pattern in Fig. 12(*c*) are accurate to a high degree, and clearly indicate that the point group of the precipitate is $6mm1_R$ when compared with Fig. 3 in Tanaka, Saito & Sekii (1983). Thus, the SMB CBED technique developed by Tanaka, Saito & Sekii (1983) appears to be preferred over the ±**g** method of Buxton *et al.* (1976) and Steeds & Vincent (1983) for determining the point group of thin specimens. The reason for this preference may be due both to theoretical considerations, whereby Friedel's law is violated only when a multiple-beam situation exists in thin specimens (Serneels, Snykers, Delavignette, Gevers & Amelinckx, 1973), as well as to the experimental limitations of keeping the electron probe stationary on the sample when a ±**g** experiment is performed. Even a slight translation of the electron beam on a thin bent specimen may be severe enough to destroy the element of centrosymmetry present in the crystal. In addition, notice that GM lines are present in the $11\bar{2}1$-type discs in the FOLZ in Figs. 11(*c*) and (*d*), and that there is no evidence in Figs. 13(*c*) and (*e*) that reflections of the type $hh\bar{0}l$, $l = 2n+1$ are forbidden. The detail within these discs is also similar to that observed for both the α-titanium

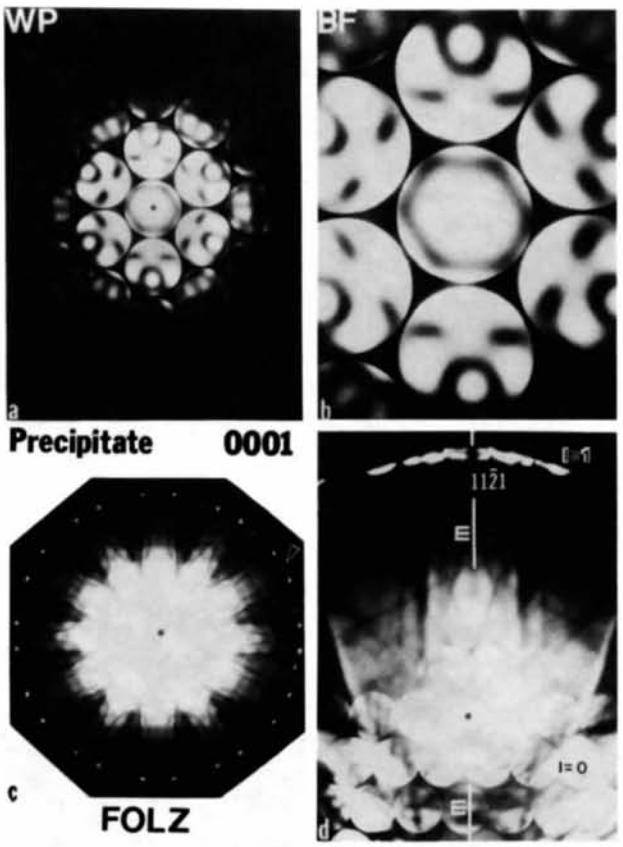

Fig. 11. CBED patterns for 120 min γ' precipitate in a [0001] orientation showing: (*a*) *6mm* symmetry in the ZOLZ, (*b*) near-sixfold symmetry within the BF disc, which is elongated because the probe is focused slightly above the precipitate surface, (*c*) *6mm* symmetry in the FOLZ, and (*d*) GM line in the $11\bar{2}1$-type FOLZ reflection at the Bragg position. The position of the optic axis is indicated by an asterisk in all of the CBED patterns. The bright ring in the FOLZ is just visible in (*c*).

and 30 min precipitate and, therefore, it can be concluded that the space group of this precipitate, which was aged for 120 min at 623 K, is also $P6_3/mmc$.

The lattice parameter along the c direction was also calculated for this precipitate from the diameter of the bright ring in the FOLZ in Fig. 11(c). By assuming that $d_{\bar{1}010} = 2{\cdot}477$ Å and using the same equation as before, the spacing was found to be $c = 4{\cdot}624$ Å. This is about 0·4% larger than the value of 4·607 Å which was determined by X-ray diffraction (Barrett & Geisler, 1940), and agrees with these results within the accuracy of the present measurements.

4. Discussion

It is worthwhile to compare the results from the present CBED space-group analyses of the γ' precipitates that were aged for 30 min at 623 K with an ordered structure proposed for the same γ' precipitates by Howe, Dahmen & Gronsky (1986). The present analyses determined the space group of these precipitates to be $P6_3/mmc$. The fact that the γ' precipitates are hexagonal close packed means that this space group represents a disordered hexagonal close-packed crystal, where the two-atom unit-cell basis is randomly occupied by either Ag or Al. The model for γ' precipitates proposed by Howe *et al.* (1986), based mainly on conventional electron-diffraction information, high-resolution electron microscopy (HREM) and image simulations, possesses long-range order among alternate basal planes, where every other plane is Ag rich, and possible short-range order within the Al-rich basal planes. As explained below, there are two possible reasons for the discrepancy between the present CBED results and the results of Howe *et al.* (1986).

First, Hren & Thomas (1963) observed that γ' precipitates are initially ordered during the early stages of growth at 623 K, but that these precipitates subsequently disorder during the later stages of growth, as evidenced by the disappearance of the 0001-type reflections. Unfortunately, these authors did not

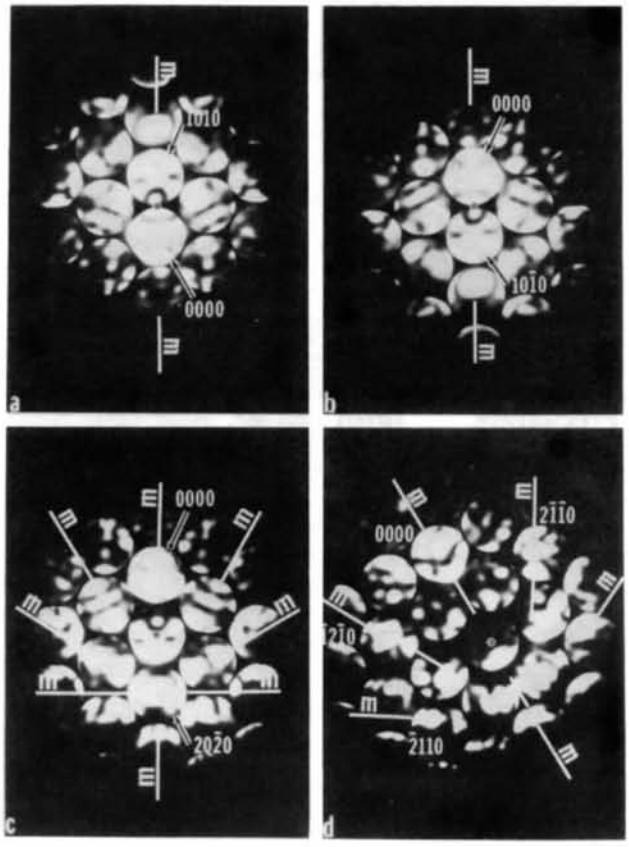

Fig. 12. CBED patterns for 120 min γ' precipitate in a [0001] orientation showing: (a) and (b) a single mirror line and 180° rotational symmetry between the $\bar{1}010$ and $10\bar{1}0$ discs located at their Bragg positions, (c) mirror lines in the six-beam pattern with the $10\bar{1}0$ disc centered on the optic axis (asterisk), and (d) symmetric excitation of the $\bar{1}2\bar{1}0$ and $2\bar{1}\bar{1}0$ reflections with mirror lines in all the $11\bar{2}0$ (and $\bar{1}010$-type) discs spaced at 30° intervals.

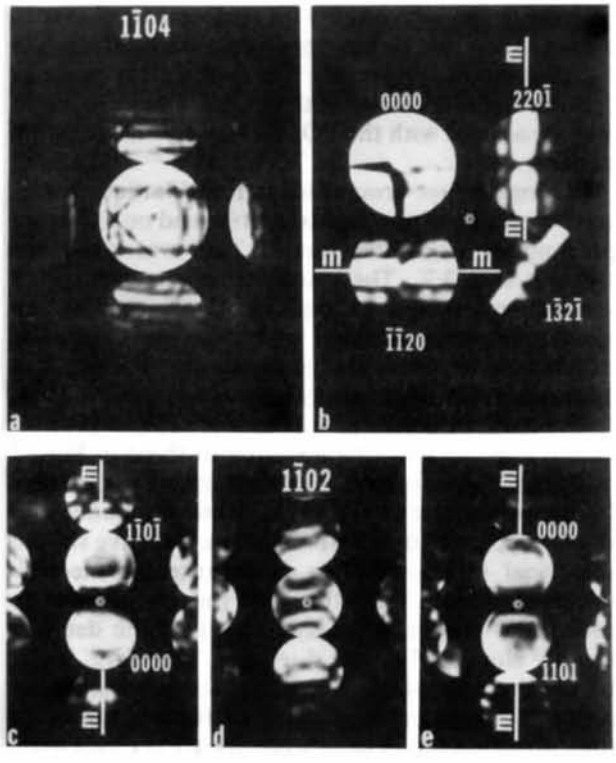

Fig. 13. (a) [$1\bar{1}04$] zone-axis pattern for 120 min γ' precipitate, (b) four-beam pattern showing mirrors in the $\bar{1}\bar{1}20$ and $220\bar{1}$ discs and the inversion symmetry in the $1\bar{3}2\bar{1}$ disc, (d) [$1\bar{1}02$] zone-axis CBED pattern which has $2mm$ symmetry but is slightly distorted due to a minor off-focus condition, and (c) and (e) opposite $\bar{1}101$-type reflections at their respective Bragg positions. Notice that the intensity fringes in the opposite $\bar{1}101$-type discs have 180° rotational symmetry, but that the faint HOLZ lines which are nearly horizontal in these discs are slightly concave down in both discs, indicating some translational symmetry.

specify the times involved for this reaction. Howe *et al.* (1986) also reported that some of the γ' precipitates in their study appeared to be disordered after aging for 30 min at 623 K, although most of the precipitates displayed some degree of long-range order among alternate basal planes. Since only the coarsest γ' precipitates from the 30 min aging treatment were suitable for analysis by CBED, it is likely that these precipitates were undergoing the disorder transformation described by Hren & Thomas (1963), thus yielding the space group $P6_3/mmc$ in the CBED analyses.

Another possible but less likely explanation for the different results is that the order was not detected in the CBED analyses due to the limited thickness of the extracted γ' precipitates analyzed. In his study of β-Si_3N_4, Bando (1983) found that CBED patterns from thin crystals were not sensitive to the weak antisymmetric part of the noncentrosymmetric crystal structure owing to the low atomic number of the N atoms. This resulted in an apparent $/m$ symmetry element in the space group because the CBED patterns depended mainly on the crystal potential of the Si atom arrangement. Since there is also a large difference between the atomic scattering factors of Ag and Al, it is possible that the CBED patterns from the thin precipitates examined in this study were not sensitive to the preferred distribution of the more weakly scattering Al atoms on alternate basal planes. However, notice that the amplitude of the 0001 reflection in Fig. 14, arising from ordering of Ag and Al on alternate basal planes, increases proportionally with the amplitudes of the other first-order beams in an ordered hexagonal close-packed precipitate. Since the precipitates from the 30 min sample were thick enough for some dynamical diffraction to cause intensity fringes within the CBED discs in the ZOLZ, they were probably only slightly thicker than one extinction distance for the first-order ZOLZ beams. Although the periodicity of the 0001 beam is almost double the periodicities of the other first-order beams, its amplitude is great enough at this thickness that it should have contributed sufficiently to the dynamic intensities to alter the CBED pattern symmetries if the precipitates were ordered. In addition, since the $/m$ symmetry element in this investigation was present in the $\langle 1\bar{1}04\rangle$ orientations where HOLZ lines were visible in the FOLZ discs for both the 30 and 120 min precipitates, there should have been sufficient dynamical interactions to reveal the actual symmetries of these specimens. Thus, this explanation does not seem as likely as the disordering reaction described above.

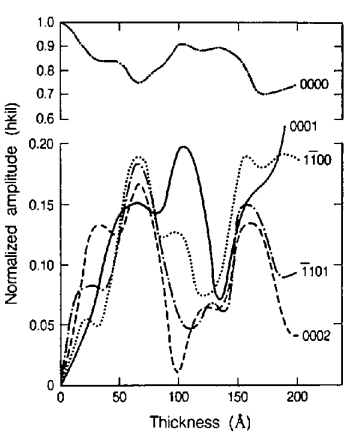

Fig. 14. Amplitudes of the forward-scattered 0000 beam and all of the first-order precipitate reflections as a function of crystal thickness for an ordered Ag_2Al γ' precipitate which contains pure Ag on the *A* basal planes and 33 at.% Ag on the *B* basal planes. The amplitudes were normalized by dividing by the sum of the amplitudes.

5. Summary

The Tanaka, Saito & Sekii (1983) method for diffraction-group determination by SMB CBED patterns appears to be less sensitive to the conditions of thin specimens than the $\pm\mathbf{g}$ technique, which is used to test for a center of symmetry in both the Buxton *et al.* (1976) and Steeds & Vincent (1983) procedures. Thus, it appears that the Tanaka, Saito & Sekii (1983) SMB method is preferred for point-group determination of thin specimens. In addition, when the specimen is thin along the electron-beam direction, the $\pm\mathbf{g}$ test for centrosymmetry is most reliable when performed at low-symmetry zone axes, since HOLZ interactions are generally stronger. In this investigation, the space group of γ' precipitates that were aged for 30 and 120 min at 623 K was determined to be $P6_3/mmc$. Since this space group represents a disordered hexagonal close-packed lattice, the CBED results do not agree with conventional diffraction data and HREM images and simulations (Howe *et al.*, 1986), which indicate that γ' precipitates aged for 30 min at 623 K are largely ordered. While it is possible that the CBED technique may not be sensitive to the order within the precipitates due to their limited thickness along the beam direction, a more likely explanation for this difference is that the γ' precipitates are undergoing a disordering reaction at 623 K as described by Hren & Thomas (1963), and that the CBED analyses sampled only the thickest and most disordered precipitates. Lattice-parameter determinations of the *c* spacing in well developed γ' precipitates performed by measuring the diameter of the FOLZ ring agree with the results of previous X-ray studies (Barrett & Geisler, 1940) within the accuracy of the technique employed.

This work was supported by the Director, Office of Energy Research, Office of Basic Energy Science,

Materials Science Division of the US Department of Energy under contract No. DE-AC03-76SF00098.

References

BANDO, Y. (1983). *Acta Cryst.* B**39**, 185-189.
BARRETT, C. S. & GEISLER, A. H. (1940). *J. Appl. Phys.* **11**, 733-739.
BOYER, H. E. & GALL, T. L. (1985). Editors. *Metals Handbook - Desk Edition*, p. 1.48. American Society for Metals, Metals Park, Ohio.
BUXTON, B. F., EADES, J. A., STEEDS, J. W. & RACKHAM, G. M. (1976). *Philos. Trans. R. Soc. London Ser. A*, **281**, 171-194.
GJØNNES, J. & MOODIE, A. F. (1965). *Acta Cryst.* **19**, 65-67.
GOODMAN, P. (1975). *Acta Cryst.* A**31**, 804-810.
GOODMAN, P. & WHITFIELD, H. J. (1980). *Acta Cryst.* A**36**, 219-228.
HENRY, N. F. M. & LONSDALE, K. (1969). Editors. *International Tables for X-ray Crystallography*, Vol. I, pp. 487-489. Birmingham: Kynoch Press.
HOWE, J. M., AARONSON, H. I. & GRONSKY, R. (1985). *Acta Metall.* **33**(4), 649-658.
HOWE, J. M., DAHMEN, U. & GRONSKY, R. (1986). *Philos. Mag.* Submitted.
HOWE, J. M. & GRONSKY, R. (1985). *Ultramicroscopy*, **18**, 83-90.
HREN, J. A. & THOMAS, G. (1963). *Trans. Metall. Soc. AIME*, **227**, 308-318.
KOHLER, V. L., SHELTON, C. G. & RALPH, B. (1983). *Proc. 41st Annual Conf. Electron Microsc. Soc. America*, pp. 258-259. San Francisco Press.
MONDOLFO, L. F. (1979). *Aluminum Alloys - Structure and Properties*, pp. 213-224. London: Butterworth.
SARIKAYA, M. & THOMAS, G. (1984). *Analytical Electron Microscopy*, pp. 97-104. San Francisco Press.
SERNEELS, R., SNYKERS, M., DELAVIGNETTE, P., GEVERS, R. & AMELINCKX, S. (1973). *Phys. Status Solidi B*, **58**, 277-292.
STEEDS, J. W. & VINCENT, R. (1983). *J. Appl. Cryst.* **16**, 317-324.
TANAKA, M., SAITO, R. & SEKII, H. (1983). *Acta Cryst.* A**39**, 357-368.
TANAKA, M., SEKII, H. & NAGASAWA, T. (1983). *Acta Cryst.* A**39**, 825-837.

Acta Cryst. (1986). A**42**, 380-386

IMPAS – A Simple Structure Determination Procedure Based on Intermolecular Patterson Vectors

BY PETER LUGER AND JOACHIM FUCHS

Fachbereich Chemie der Freien Universität Berlin, Takustrasse 6, *D*-1000 *Berlin* 33, *Federal Republic of Germany*

(*Received* 15 *February* 1985; *accepted* 22 *April* 1986)

Abstract

A computer method for interpreting Patterson functions of crystals belonging to space groups of higher symmetry than *P*1 is described. A table of all Patterson peaks in the entire cell is initially searched for vectors between symmetry-related atoms. Such 'generalized Harker vectors' are identified not only by known symmetry-fixed components, but also by statistical criteria based on a systematic search for pairs of vectors which relate additional atoms to the pair involved in the generalized Harker vector. Subsequent searches, using the same basic principle, are carried out to find additional atoms. Pairs of vectors, whose components add up to the previously established Harker vector, indicate newly found atom positions after appropriate transformations into crystal space. The correctness of these atom positions can be further tested by applying all symmetry operations of the space group in question and looking for a complete set of related vectors. In contrast to many other Patterson search methods no information about known molecular fragments is requested. Also described are four structures which were solved with the *IMPAS* procedure following unsuccessful attempts to solve them by direct methods.

0108-7673/86/050380-07$01.50

© 1986 International Union of Crystallography

Introduction

50 years ago, Patterson (1934) introduced the Fourier transform of the squared structure amplitudes as one of the most important crystallographic functions into the literature. For more than 30 years the deconvolution of the Patterson function was the major procedure for solving the crystallographic phase problem. Several techniques were developed [superposition method (Jacobson, 1966), image-seeking functions (Buerger, 1959), *Faltmolekülmethode* (Huber & Hoppe, 1965), *etc.*] mainly aimed at searching for suitable intramolecular Patterson vectors.

In the last decade 'direct methods' have superseded Patterson methods as the major tool in solving crystal structures. Among the organic and organometallic structures published in 1982 the phase problem was solved with direct methods in 72% of the cases, and with Patterson methods in 28% (de Ranter, 1984). Nevertheless, a number of structural problems remain, where direct methods fail or are successful only after overcoming considerable difficulties. These problems occur in a few unsuitable space groups such as *P*1 or *C*2, in cases with high internal molecular symmetry (mainly observed in inorganic